

Supporting Information

Reversible Electrochemical Conversion from Selenium to Cuprous Selenide

Sean K. Sandstrom,^a Heng Jiang,^a Marcos Lucero,^b Yunkai Xu,^a Trenton C. Gallagher,^a Mengyuan Cao,^a Zhenxing Feng,^{b,*} Xiulei Ji^{a,*}

^aDepartment of Chemistry, Oregon State University, Corvallis, OR 97331, USA.

^bSchool of Chemical, Biological, and Environmental Engineering, Oregon State University, Corvallis, OR 97331, USA.

Email: david.ji@oregonstate.edu, zhenxing.feng@oregonstate.edu

Experimental Procedures

Preparation of Materials:

The selenium/KB composite was prepared by a melt-diffusion method by first ball milling selenium powder (Sigma Aldrich, 100 mesh, >95%) with Ketjenblack (KB) carbon in a 3:1 mass ratio at a rotation speed of 400 rpm for 3 hours. Subsequently, the ball-milled Se/KB mixture was pressed into a pellet and heated overnight at 230 °C in a crucible inside a muffle furnace. The S/KB composite was prepared in an identical manner except for a temperature of 150 °C being used as the melt-diffusion temperature due to the lower melting point of sulfur.

Physical Characterization of Materials:

X-ray diffraction (XRD) was measured using a Rigaku Ultima IV Diffractometer with Cu K α irradiation ($\lambda=1.5406$ Å) at a scan rate of 1 degree per minute. Thermogravimetric analysis (TGA) was conducted under argon atmosphere at a ramp rate of 10 °C per minute using a SDTQ600 Thermal Analyzer. High-angle annular dark field scanning transmission electron microscopy (HAADF-STEM) images and the associated energy dispersive X-ray (EDX) spectra were collected using an FEI Titan 80-200 TEM/STEM. Brunauer-Emmett-Teller (BET) analysis was done via a Micromeritics Tristar II surface area and porosity analyzer using N₂ at 77.3 K. X-ray absorption near-edge structure spectroscopy (XANES) of the Cu K-edge was obtained via the Stanford Synchrotron Radiation Lightsource (SSRL) at the SLAC National Accelerator Laboratory at beamline 11-2. XAS measurement were conducted in transmission mode using ion chambers to detect the Cu transmission signal. The XAS data processed using Athena background subtraction and post-edge normalization. Artemis was utilized to quantitatively analyze the extended X-ray absorption fine structure (EXAFS). Scattering paths for EXAFS shell fitting were obtained from the crystal structure of the standards.

Electrochemical Characterization:

The Se/KB-75 electrodes were prepared by mixing the Se/KB-75 nanocomposite and polyvinylidene fluoride (PVdF) with a mass ratio of 9:1 in N-methyl-2-pyrrolidone (NMP). The resulting homogeneous slurry was then cast onto carbon paper current collectors and dried at 70 °C overnight. The S/KB-75 electrodes were prepared in an identical manner. The active mass loading of Se (or S) in the electrodes was approximately 2.05 mg/cm². The free-standing film electrodes used for obtaining the *ex-situ* XRD patterns were composed of 70 wt.% Se powder, 20 wt.% Super C65 carbon, and 10 wt.% polytetrafluoroethylene (PTFE) binder. The free-standing film electrodes had a Se mass loading of ~20.5 mg/cm².

All electrochemical tests were conducted using Swagelok three-electrode cell configurations. The Cu²⁺/Cu⁺ storage performances of Se/KB-75 and S/KB-75 were obtained using either Se/KB-75 or S/KB-75 as the working electrode, and metallic copper as the counter and reference electrodes. Whatman™ filter papers were used as the separator. Galvanostatic charge/discharge (GCD) measurements were obtained using a LANDT Battery Test System CT3002A. Cyclic voltammetry (CV) tests were performed on a VMP-3 multi-channel workstation.

Calculations of the Volume Expansions of Conversion Between Se and Cu₂Se:

Calculations were done to determine the maximum selenium content that can fit into the pores of KB and still allow for the volume expansion associated with copper hosting. Starting with the pore volume of KB (~2.69 cm³/g) obtained from BET analysis and the density of Cu₂Se (6.84 g/cm³), we calculated that 18.4 g is the theoretical maximum mass of Cu₂Se (the final discharged product) that can be contained inside the pores of 1 g of KB. From this mass, we then calculated the theoretical limit of Selenium that can be encapsulated in pores of KB and still allow for full conversion to Cu₂Se as 7.05 g of Se for every 1 g of KB. From our experimental results, we found that a mass ratio of ~4:1 Se:KB was the maximum Se content that could be encapsulated inside the carbon pores via the melt-diffusion technique.

Results and Discussion

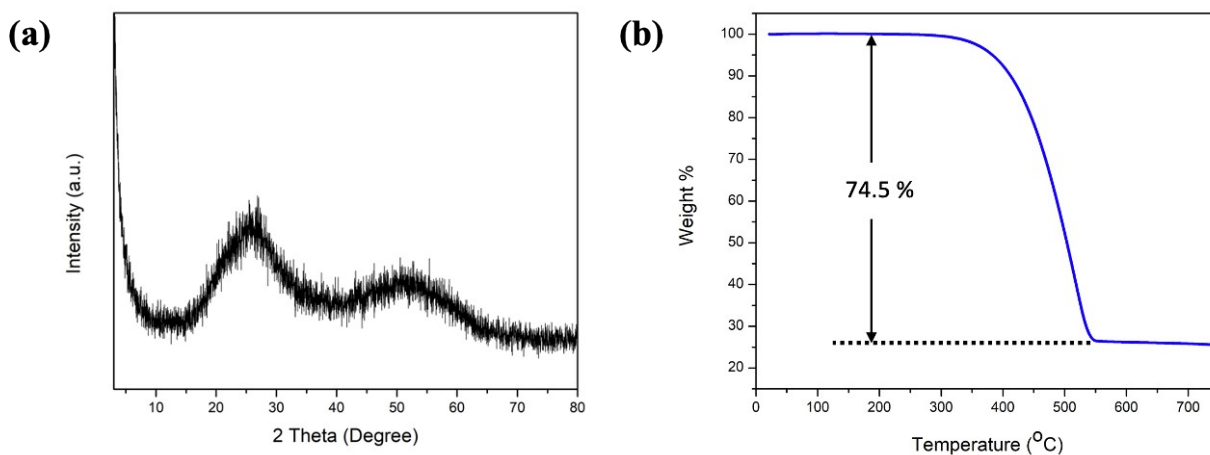


Figure S1. Material characterization of the Se/KB-75 composite. (a) X-ray diffraction pattern obtained at a scan rate of 1 degree per minute. (b) Thermogravimetric analysis under Ar atmosphere at a ramp rate of 10 °C per minute. The amorphous XRD pattern reveals the successful encapsulation of selenium within the carbon nanopores. The ~75% mass loss seen in the TGA reveals that the majority of the mass of selenium was retained within the composite.

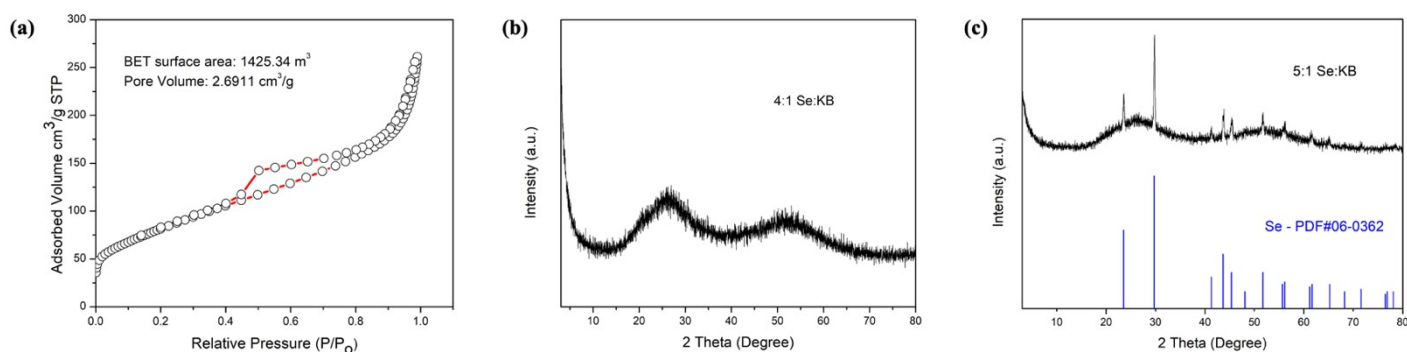


Figure S2. Determination of the maximum selenium content capable of being encapsulated in the pores of KB via the melt-diffusion technique. (a) N_2 adsorption/desorption isotherm of KB with the associated pore volume used in determining the theoretical maximum Se content. XRD patterns of the Se/KB nanocomposites prepared with (b) 4:1 and (c) 5:1 Se:KB mass ratios. The pore volume of KB was used to determine a theoretical maximum Se loading of ~ 87.6 wt.%. The broad peaks at $\sim 26^\circ$ and 53° in the XRD pattern of the 4:1 Se:KB composite are attributed to the (002) and (101)/(010) planes of Ketjenblack carbon. XRD patterns show the unsuccessful encapsulation of Se inside pores of KB at a mass ratio of 5:1, where the peaks of elemental Se have been indexed.

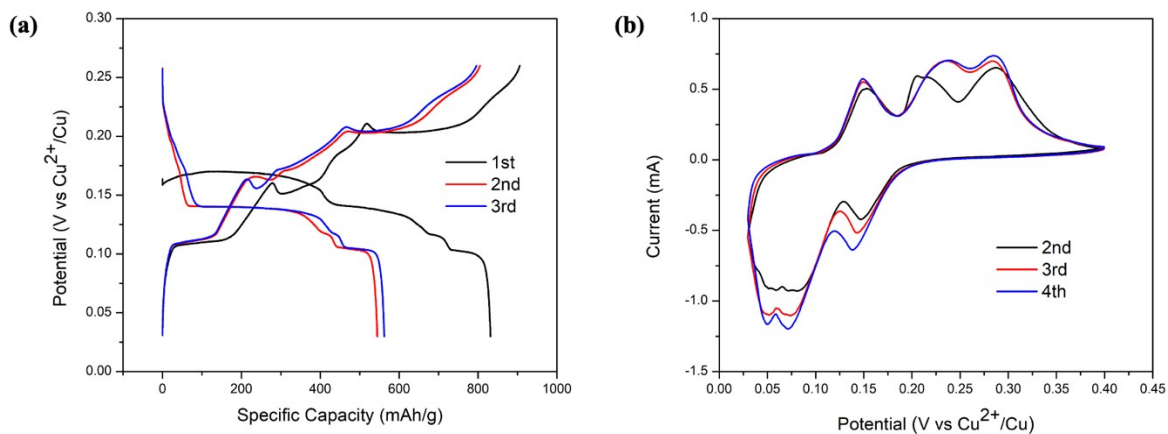


Figure S3. Electrochemical performance of selenium ground with KB. (a) GCD curves obtained at 100 mA/g and (b) CV curves obtained at a scan rate of 0.03 mV/s.

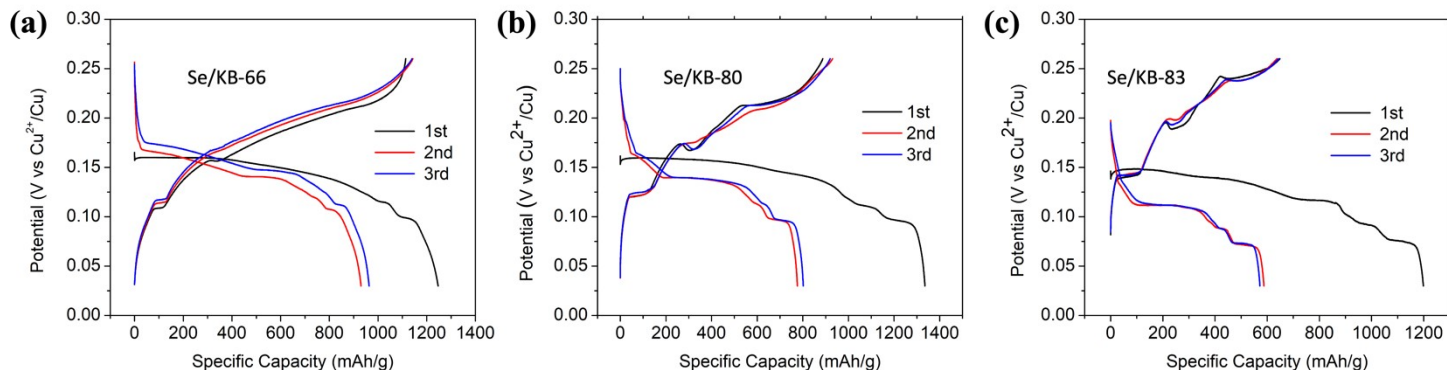


Figure S4. GCD potential profiles obtained at a current rate of 100 mA/g for the Se/KB composites with (a) 66, (b) 80, and (c) 83 wt. % selenium. As can be seen from the GCD profiles, the overpotential increases as the Se content increases. The less desirable profiles with higher Se content may be ascribed to lower conductivity, less structural stability during the conversion reactions, and an increased polyselenide shuttling effect when the Se content is not entirely confined within the KB pores.

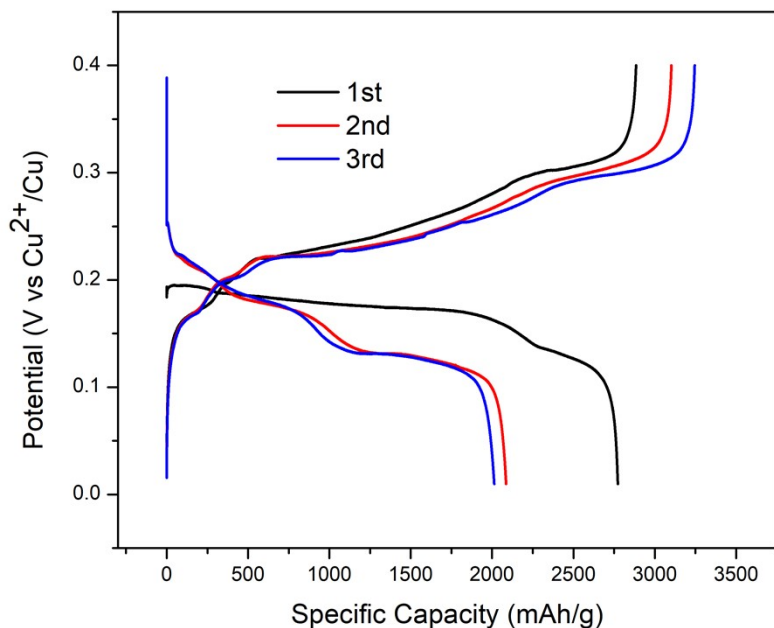


Figure S5. First three GCD cycles of the S/KB-75 composite electrode in a potential window from 0.01 to 0.4 V vs Cu^{2+}/Cu obtained at a current rate of 100 mA g^{-1} .

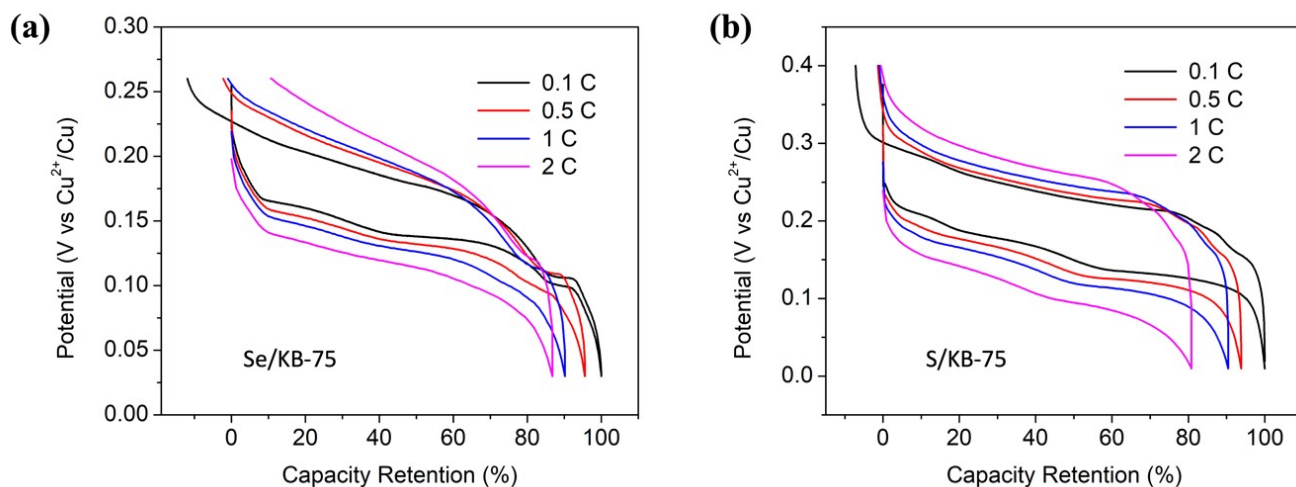


Figure S6. Rate performance comparison of the (a) Se/KB-75 and (b) S/KB-75 composite electrodes. Each C rate is determined based on the theoretical four-electron capacity of Se or S. A capacity retention of $\sim 87\%$ and $\sim 81\%$ was observed in going from 0.1 C to 2 C for the Se/KB-75 and S/KB-75 electrode, respectively. The polarization increased by 49 mV and 83 mV for the Se/KB-75 and S/KB-75 electrodes, respectively, in changing the rate from 0.1 C to 2 C.

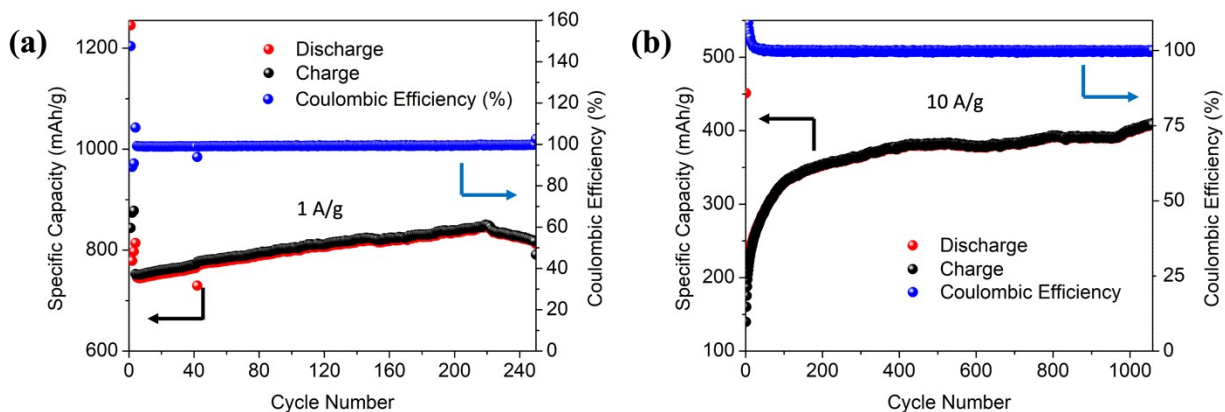


Figure S7. Cycling performance of the Se/KB-75 electrode at the current rates of (a) 1 A/g and (b) 10 A/g. For both current rates, the capacity steadily increases in the initial cycles, which indicates a continued activation process of the Se/KB-75 electrode. The initial 3 cycles of the cycling performance at 1 A/g were done at 100 mA/g to further condition the electrode before cycling at 1 A/g.

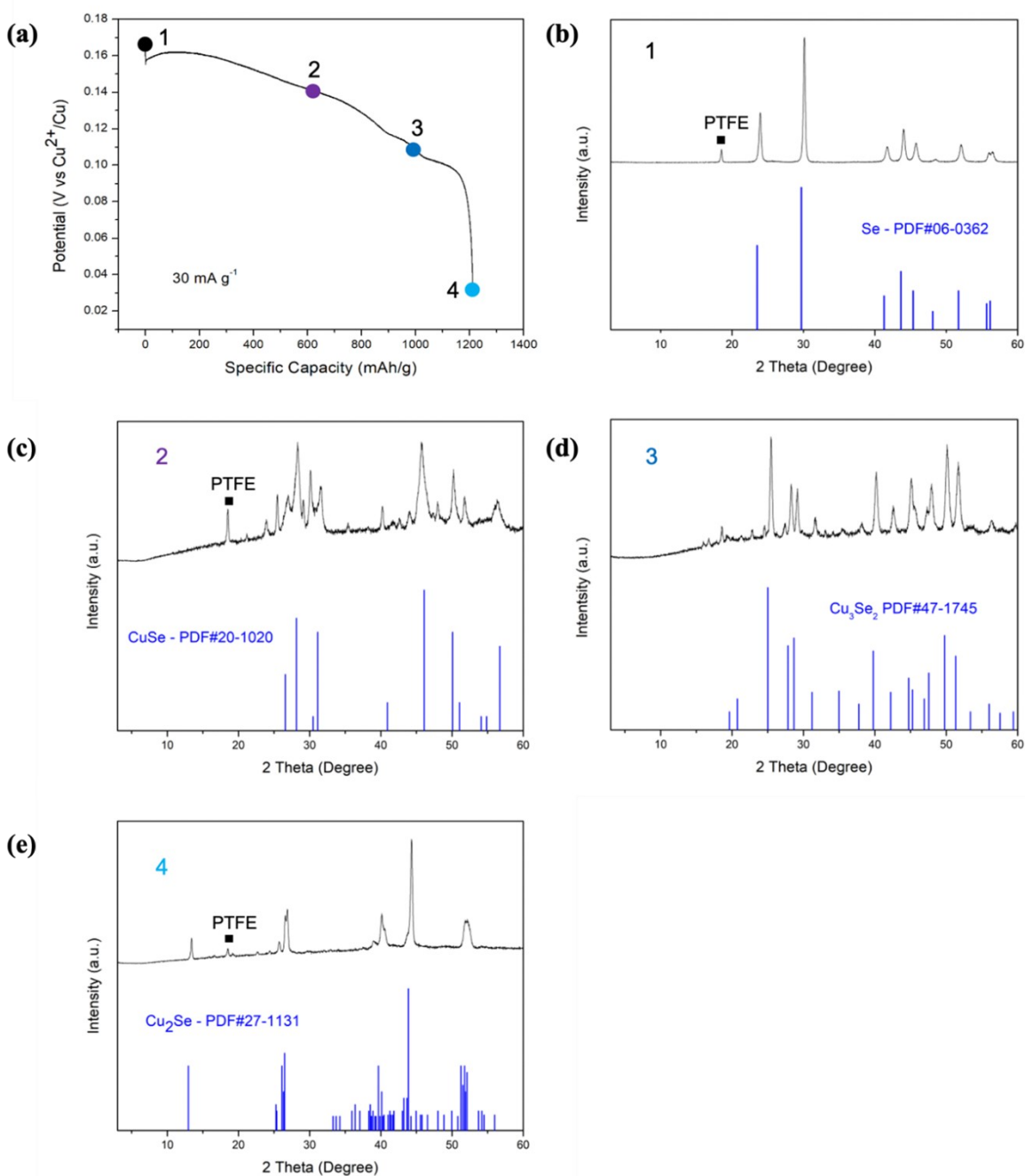


Figure S8. *Ex situ* XRD patterns of the Cu-Se RIC free-standing film electrode. (a) Representative galvanostatic discharge curve of the free-standing film electrode at a current rate of 30 mA g^{-1} . (b) XRD pattern of the pristine Se free-standing film electrode. XRD patterns obtained at (c) position 2 (~50% SOC), (d) position 3 (~75% SOC), and (e) position 4 (fully discharged) on the discharge curve. Peaks that correspond to the PTFE binder in the free-standing film XRD patterns are marked with a square. As can be seen, the XRD patterns are indexed indicating a sequential four-step conversion reaction via $\text{Se} \rightarrow \text{CuSe} \rightarrow \text{Cu}_3\text{Se}_2 \rightarrow \text{Cu}_2\text{Se}$.

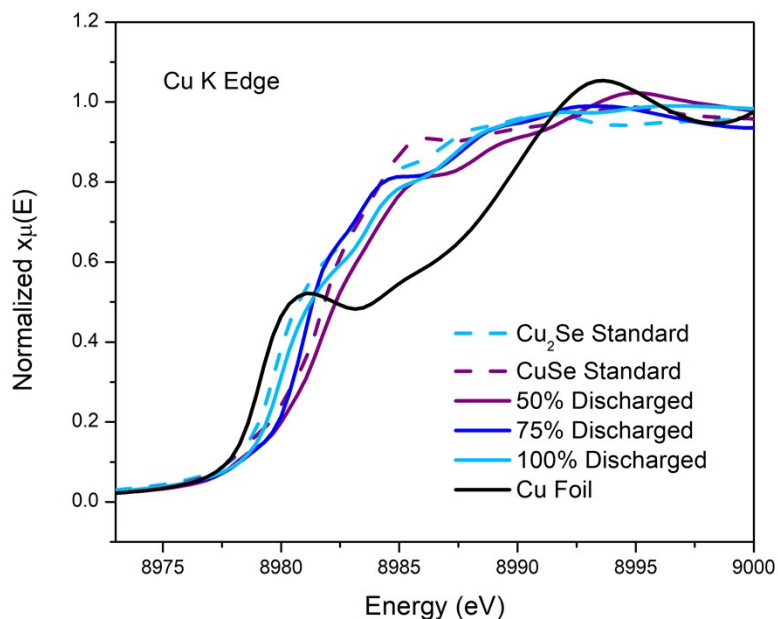


Figure S9. Normalized XANES of the Cu K-edge spectra of Cu-Se electrode obtained at different SOC and the CuSe, Cu₂Se, and Cu foil standards.

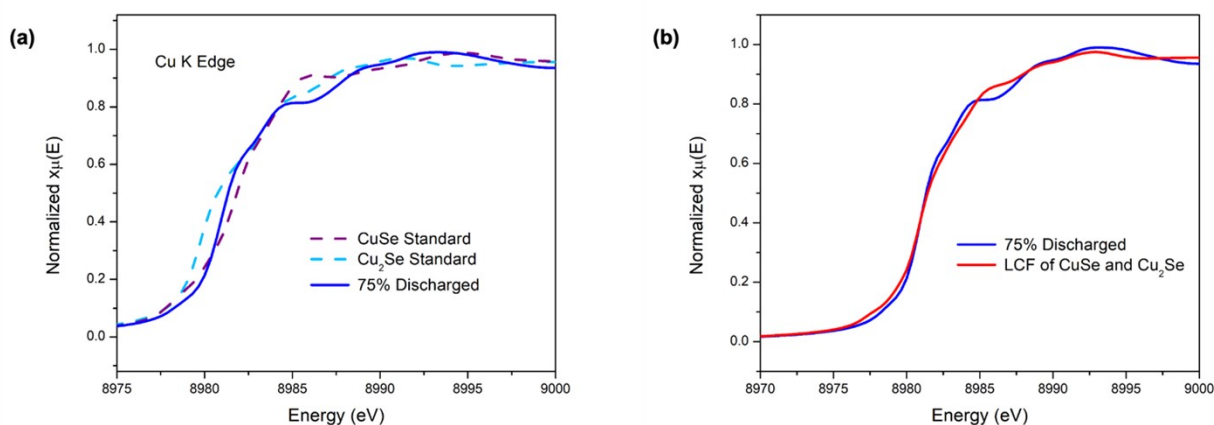


Figure S10. XANES analysis of the 75% discharged Cu-Se electrode. (a) Comparison of the normalized XANES of the Cu K-edge spectra of the Cu-Se electrode at 75% SOC and the CuSe and Cu₂Se standards. (b) Comparison of the linear combination fit obtained using the CuSe and Cu₂Se standards. The position of the Cu K-edge spectra of the 75% discharged sample being in between the spectra obtained for the CuSe and Cu₂Se standards indicates the formation of a mixed oxidation state Cu⁺/Cu²⁺ Cu₃Se₂. The fact that the linear combination fitting obtained using the CuSe and Cu₂Se does a good job of reproducing the K-edge of the 75% discharged sample further indicates the mixed Cu oxidation state of the 75% discharged sample.

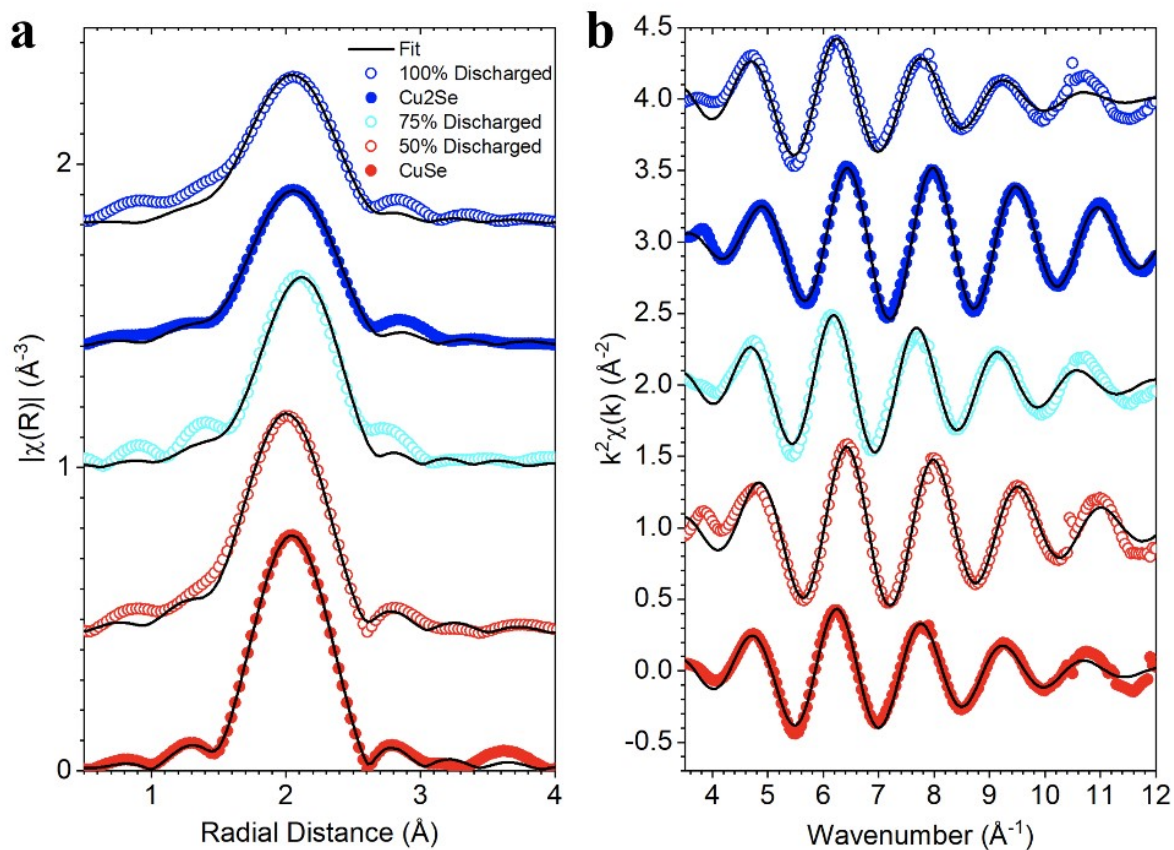


Figure S11. Model based fitting of (a) Fourier transformed and (b) k-space EXAFS spectra for the Cu-Se electrode obtained at 50%, 75%, and 100% SOC and the CuSe and Cu₂Se standards.

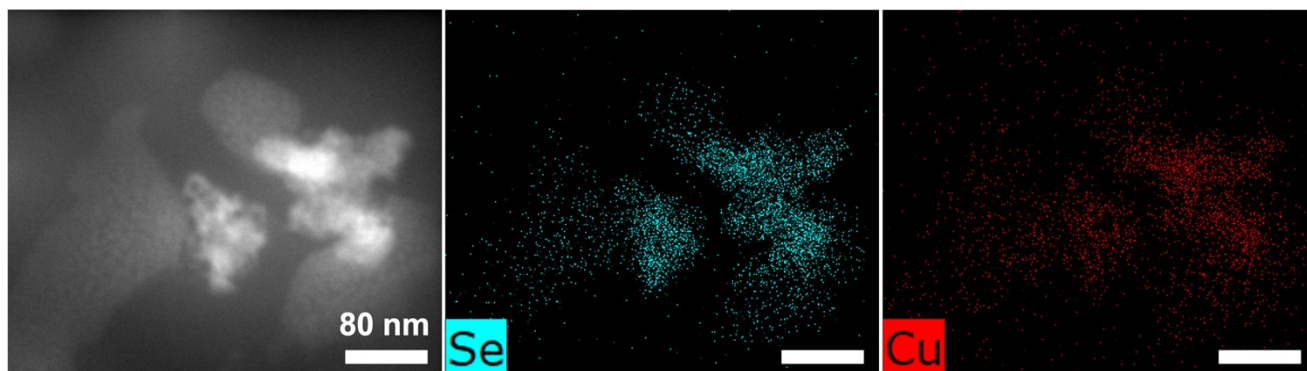


Figure S12: High angle annular dark field scanning transmission electron microscopy (HAADF-STEM) image of the fully discharged Cu-Se composite electrode with corresponding EDX mappings of the Se and Cu content

Table S1: Fitting parameters of the EXAFS spectra of standards (Cu_2Se , Cu_3Se_2 , CuSe) and the electrode materials at different SOC. CN: coordination number; R: distance; σ^2 : mean-square disorder.

Sample	$\text{CN}_{\text{Cu-Se}}$ (Theoretical)	$\text{CN}_{\text{Cu-Se}}$ (Calculated)	$\text{R}_{\text{Cu-Se}}$ (Å) (Theoretical)	$\text{R}_{\text{Cu-Se}}$ (Å) (Calculated)	σ^2 (Å ³)	R-factor
Cu_2Se	4	4.00 ± 0.49	2.51	2.43 ± 0.01	0.015 ± 0.001	0.007
Cu_3Se_2	4	-	2.46	-		
CuSe	3	3.03 ± 0.16	2.44	2.38 ± 0.01	0.0077 ± 0.001	0.002
50 % SOC (CuSe)	-	3.21 ± 0.37	-	2.36 ± 0.01	0.011 ± 0.001	0.010
75% SOC (Cu_3Se_2)	-	3.99 ± 0.78	-	2.45 ± 0.01	0.014 ± 0.002	0.02
100 % SOC (Cu_2Se)	-	4.36 ± 1.0	-	2.42 ± 0.02	0.017 ± 0.003	0.02